SATURNUS: The UCLA Compact Infrared Free-Electron Laser Project

J.W. Dodd, F. Aghamir, W.A. Barletta, D.B. Cline, S.C. Hartman, T.C. Katsouleas, J. Kolonko, S. Park, C. Pellegrini, J.-C. Terrien
Center for Advanced Accelerators, Department of Physics, U.C.L.A., Los Angeles, CA, 90024-1547

J.G. Davis, C.J. Joshi, N.C. Luhmann, D.B. McDermott
Department of Electrical Engineering, U.C.L.A., Los Angeles, CA 90024-1594

S.N. Ivanchenkov, Yu.Yu. Lachin, A.A. Varfolomeev
I.V. Kurchatov Institute of Atomic Energy, Moscow, 123182, U.S.S.R

ABSTRACT

Saturnus is an infrared FEL operating in the 10 μm wavelength region, driven by a compact 20 MeV linac with a photoinjector, under construction at UCLA. The 1.5 cm period, 0.6 T peak field undulator is being built at the Kurchatov IAE. The FEL is designed to operate primarily in the self amplified spontaneous emission mode. We plan to study the start-up from noise, optical guiding, saturation, sidebands and superradiance, with emphasis on the effects important for future short wavelength operation of FEL's. The photoinjector follows closely the Brookhaven design. Electrons are injected into an accelerating section based on the Plane-Wave Transformer design developed by Swenson at SAIC. Simulation of the linac and FEL show a gain length of 10 cm., and a saturation power of 50 MW.

1. INTRODUCTION

A compact 20 MeV linac with an RF laser-driven electron gun is being built at UCLA. This linac will be used to study the production of high-brightness electron beams, and to drive a high gain, 10.6μm wavelength FEL amplifier, capable of operating in the SASE mode. Saturnus will use a 1.5cm period, 6.5kG peak Field undulator developed and built at the Kurchatov Institute of Atomic Energy. A list of the main FEL, undulator and linac design parameters are given in Table 1, and a layout of the system is shown in fig. 1.

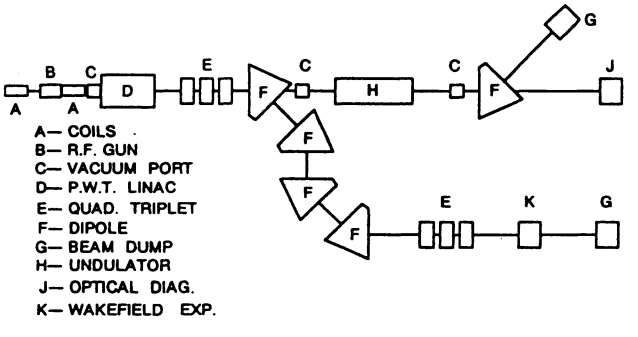

Figure 1. Layout of the UCLA free-electron laser. Two beam-lines are shown. The straight path transits the undulator. The bent path allows beam diagnosis and an auxiliary means to magnetically compress the electron bunches.

Saturnus will mainly study FEL physics in the high-gain regime, including start-up from noise, optical guiding, sidebands, saturation, and superradiance, with emphasis on the effects important for future short wavelength operation of FEL's.[1] For the electron beam we will study

ways to improve the beam brightness and peak current. We will have two beam lines, one leading straight into the undulator, the other designed for beam diagnostic and longitudinal bunch compression. This second beam line will also be used for other particle beam physics experiments, including plasma wakefield acceleration.[2]

Table 1. Saturnus design parameters.

ELECTRON BEAM	
Energy, nominal	16.5MeV
Energy spread, r.m.s.	0.2%
Peak current	200A
Klystron frequency	2.865GHz
Pulse repetition rate	5Hz
Macropulse duration	3.5μsec
micropulse duration, r.m.s.	≈1.6psec
Charge per bunch	≈1nC
Normalized emittance, r.m.s.	15mm-mrad
UNDULATOR	
Drift tube I.D. within undulator	4mm
Period	1.5cm
Length	60cm
Fixed gap between pole pieces	5mm
Field on axis	5.5kGauss
FEL OUTPUT RADIATION	
Wavelength	10.6μm
Gain length	10cm
Saturation length	130cm
Peak saturated power	50MW

2. PHOTOEMITTING RF ELECTRON GUN

The electron injector is based on the photocathode, RF gun designed at Brookhaven National Lab.[3] The cathode will be illuminated at 70° or 2°30′ off-axis. The idea to use photocathodes in RF electron guns originated at Los Alamos National Lab.[4] The gun consists of one and one-half cavity cells operating in the π-mode and resonating at 2.856 GHz. Powered by 5MW extracted from a 25MW SLAC klystron, the electron gun can produce a beam energy approaching 4.5 MeV. The gun is followed by a solenoid to focus the beam into the accelerating section.

Photoemission is initiated by irradiating the cathode with a frequency quadrupled light pulse from a Nd:YAG/Glass laser. Two sapphire viewports are oriented 70° from the electron beam axis and situated symmetrically about the line perpendicular to the planar cathode's surface. Initially a copper cathode will be used (quantum efficiency $\geq 10^{-5}$). For the linearly polarized laser beam, off-axis incidence preferentially enhances the photoemission by providing an electric field component parallel to the axis. For a LaB_6 crystalline photocathode, twice the amount of photoemission at 70° has been observed compared to axial illumination at 0°.[5] For long pulse studies (≥ 30psec.) the second port will be used to align the injected pulse from the first port.

For short pulse studies (≤ 3 psec.), off-axis illumination causes a time delay across the breadth of the laser pulse when it strikes the cathode surface, thereby producing a much longer electron pulse. To preserve an ultra-fast electron pulse, a mirror placed between the gun and the linac, near the electron beam axis, will be used to illuminate the cathode. The time delay diminishes to about one picosecond.

2.1. RF Gun Simulations:

Computer simulations of the electron gun have been done using the SUPERFISH[6] code to model the electric fields within the $1\frac{1}{2}$ cells and the PARMELA code, as extended by McDonald[7] to include photocathodes, to model the electron beam dynamics. The r.m.s. beam size along the x or y-axis versus the distance downstream from the photocathode surface is shown in fig. 2, with the focusing solenoid field "on" (focusing field strength ≈800 Gauss). Without the focusing coil, the beam out of the gun is strongly divergent and only a small part of it would propagate through the accelerating section. For the parameters in Table 1, PARMELA yields a normalized emittance along the x or y-axis of 15mm-mrad at the exit of the focusing solenoid.

Fig. 3 shows the longitudinal phase-space, with an energy spread of about ±0.5% and a phase acceptance corresponding to a pulse

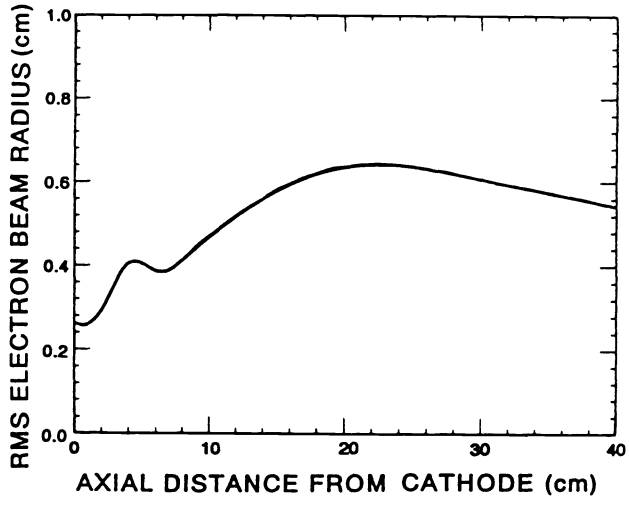

Figure 2. PARMELA simulation of the electron beam radius propagating through the gun and focusing solenoid. The exit of the gun is 8cm downstream from the cathode. The end of the focusing solenoid is 32cm from the cathode surface.

Table 2. Solid-state laser performance values.

STAGE	λ_{OUT}	PULSE DURATION	PULSE ENERGY
YAG OSCILLATOR (76.16MHZ PRF)	1.064μm	80psec	0.3μJ
REGEN. AMP (5HZ PRF)	1.064μ	70psec	15mJ
TWICE DOUBLED	266nm	50psec	2mJ
ADD FIBER & GRATING PAIR	266nm	≥2psec	0.25mJ

duration of about 4psec. The incident laser pulse shall be on the order of 2-4psec.

2.2. Nd:YAG/GLASS Laser:

The ultraviolet fourth-harmonic of a high-powered Nd:YAG laser system illuminates the photocathode. The solid-state laser system contains: (1) a Coherent®, Antares™ Nd:YAG laser oscillator, 22W, mode-locked at 38.08MHz, (2) a Continuum®, model RGA-44-5, Nd:Silicate Glass regenerative amplifier, operating at a 5Hz, (3) an optical fiber and diffraction grating pair to provide pulse chirping and compression, respectively, and (4) two frequency doubling KD*P crystals. Additional optics, power

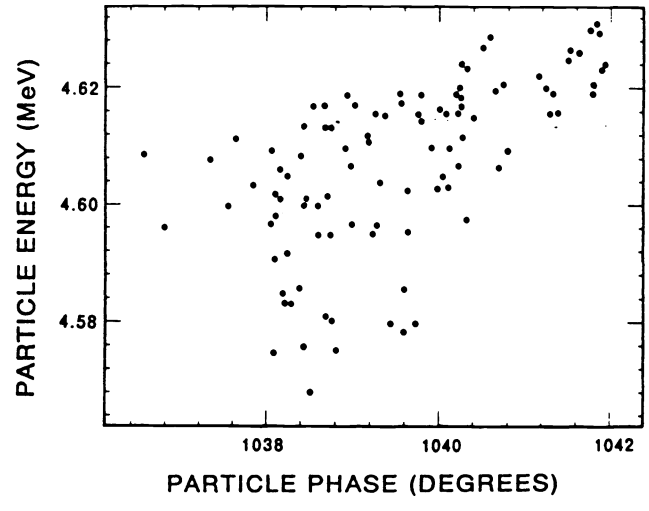

Figure 3. Longitudinal phase-space at the exit of the solenoid.

isolators, mirrors, etc., complete the system. Table 2 specifies performance values for the solid-state laser system. To produce a train of electron bunches sufficient for FEL oscillation (100-200 pulses separated by 13.1nsec.), two more amplification stages after the regenerative amplifier are required.

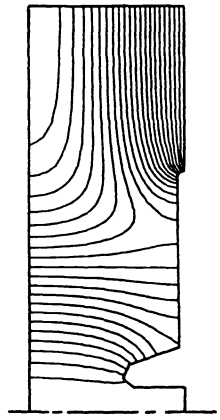

Figure 4. Electric field pattern for a quarter-cell of the prototype plane-wave transformer linac.

3. PLANE-WAVE TRANSFORMER LINAC

The linac is the prototype plane-wave transformer structure designed by Swenson.[8] Capable of achieving 20MeV electron energies within a distance of half-a-meter, the prototype consists of a cylindrical tank with eight washers placed along the axis. The distance between each washer is evenly spaced. Half this distance is the spacing given between the end washer and the respective end-wall of the tank. The space between the outer diameter of the tank and the washer array supports a TEM-style "coaxial" standing wave. The washer array is equivalent to the "center conductor." The plane-wave traveling back and forth along the structure couples power into the "cells" producing a TM_{02}-like mode between the washers. This is equivalent to a periodically loaded coax-cable that transforms the transverse field of the TEM standing plane-waves into a longitudinal electric field along the axis ready to accelerate particles. A SUPERFISH simulation of the PWT linac's electric field shows in fig. 4 the longitudinal orientation on axis as well as the transition from the outer-lying transverse fields.

4. HYBRID UNDULATOR

The hybrid undulator was designed and constructed at the Kurchatov Institute of Atomic Energy in the U.S.S.R. The primary magnetic flux is provided by C-shaped iron (Vanadium-permendur is an optional material.) yokes where between the poles thin blocks of neodymium-iron-boron magnets are placed to provide additional magnetic flux along the undulator axis. The field strength is also adjusted by moving the thin Nd-Fe-B blocks towards or away from the axis on a set-screw mount. Fig. 5 is a schematic diagram of the Kurchatov undulator. The initial assembly

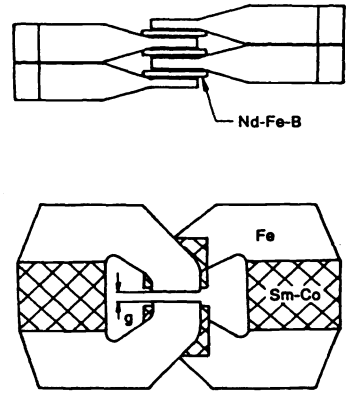

Figure 5. The Kurchatov hybrid undulator (g = 5mm).

will have forty periods with each period being 1.5 cm. The gap distance between the "yoke" pole-pieces is fixed at 5mm. A mock-up of the undulator having over five periods was measured and yielded an on axis peak field of 6.5kGauss. A computer simulation using the TOSCA[9] code gives similar results of approximately 6kGauss on axis.

5. ELECTRON BEAM DIAGNOSTICS

5.1. Current and Position:

The charge per bunch will be first measured using a Faraday cup to collect the electron pulse on an integrating RC circuit. Along with the electron gun, the electron beam position diagnostic is based upon a design used on ATF at BNL. Three monitors will be used—two to align the electron beam through the undulator and one to position the beam as it enters the emittance selecting dipole pair. Each monitor consists of four stripline electrodes placed symmetrically around the electron beam, inside and electrically isolated from the vacuum vessel via ceramic, vacuum feed throughs. Each slightly curved stripline electrode is 8.5 cm. long and 1.1 cm. wide. The signal induced on each stripline is integrated in a preamplifier. The total signal induced on the four striplines is proportional to the total charge in a bunch. The difference of the signals between two diametrically opposed striplines determines the relative position of the electron bunch from the geometric center of the four striplines. The sum and difference signals are subsequently sent to a heterodyne receiver with local oscillator at 2.856GHz, in order to rectify the signal sent to the preamplifier. Each microbunch generates a positive and negative signal of equal magnitude on the electrode, separated by twice the transit time of the electrode's length (i.e., 500psec).[10] The heterodyning process reverses the polarity of the second pulse, therefore the net integrated charge is doubled instead of cancelled in the preamp.

5.2. Emittance, Energy Spread, and Overall Energy:

The beam emittance will be measured using a technique similar to that developed at ATF.[11] A phosphor screen is placed to intercept the electron beam. The spot size is reflected into an optical camera. The emittance can be unfolded from the comparison of the spot sizes at two different settings of the beam transport system.[12]

In the dispersive region, between the dipole magnets, the energy and energy spread of the electron beam can be measured by placing the phosphour screen at the central location of the beam focus. Since the beam emittance is expected to be low, an angular spread in the spot size at the focus (as seen on the charge-coupled camera viewing the phosphour screen) can by and large be attributed entirely to the energy spread in the beam. The average energy of the beam can be determined from locating the centroid of the electron spot as seen on the phosphour screen and comparing to the calculated trajectory.

5.3. Temporal Pulse Duration:

The time duration of the electron pulse will be measured by passing the electron beam through a thin plate of dielectric material, then sweeping the Cerenkov radiation thereby produced, on the picosecond time scale using a streak camera.

6. FEL OUTPUT: DIAGNOSIS AND SIMULATIONS

The FEL's output wavelength will closely match the 10.6μm radiation which CO_2 lasers produce, simplifying the diagnosis of the output radiation. For cryogenic infrared detectors sensitive to 10μm wavelengths, the expected power output from spontaneous emission in the FEL is marginally detectable. For 1nC charge per bunch, $1.2 \cdot 10^7$ photons per micropulse are expected from spontaneous emission within an angle $\Theta = 1/(\gamma \cdot \sqrt{N})$ and a line width $1/(2N)$. This amount can be detected directly. For smaller charges one can integrate the signal over many pulses.

The FEL performance in SASE is evaluated using the TDA code developed by Tran and Wurtele at MIT.[13] Using the parameters of Table 1, TDA predicts a gain length of 10cm, with a saturation power of 50MW. This assumes that the full 200A peak current is achievable. TDA also assumes free-space propagation, whereas our 0.2mm wide electron traverses the undulator inside a ≈4mm inner diameter drift tube. A calculation employing complete waveguide modes may modify these results. Fig. 6(a) graphs the power versus distance along the undulator as projected by TDA. Fig. 6 uses an input power of 40mW, corresponding to the spontaneous radiation emitted in one gain length, within the angle and linewidth given above. This radiation is assumed to be focused to a spot radius $(\lambda L_{UNDUL.})^{1/2}/4\pi$ at the centre of the first gain length.

Fig. 6(b) plots the calculated r.m.s. optical beam radius versus the distance along the undulator. Notice that once growth occurs the optical beam collapses and remains in the vicinity of the electron beam as it propogates down the entire undulator. This is indicative of optical guiding.

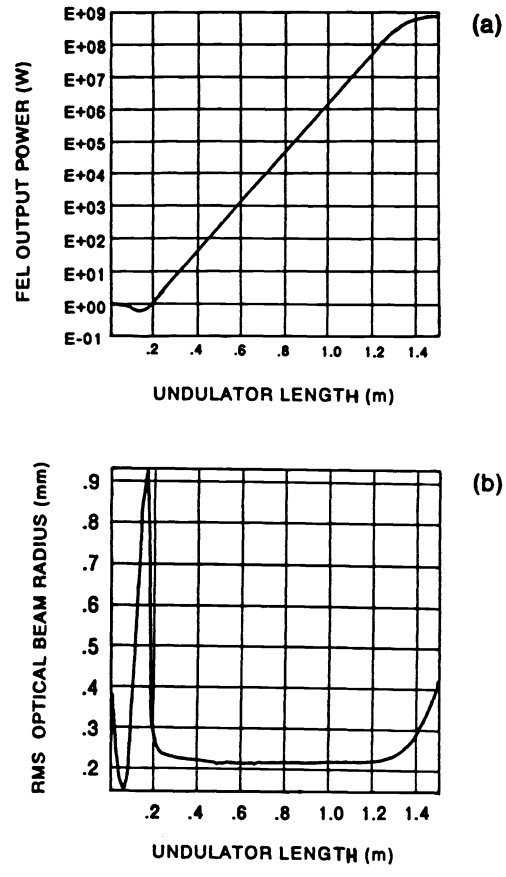

Figure 6. TDA simulations of SASE using the parameters in table 1: (a) power growth through the undulator and (b) radius of the optical beam within the undulator. Optical guiding is evident since the optical beam remains confined near the electron beam, once power growth predominates.

7. ACKNOWLEDGEMENTS

Our group appreciates the help received from H. Kirk, K. Batchelor, J. Xie, J. Sheehan, G. Bennett, J. Wurtele, M. Allen, G. Loew, M. Baltay, and H. Hoag. This work is supported by DOE Grant No. DE-FG0-90ER-40565.

8. REFERENCES

[1] C. Pellegrini, *Nucl. Instr. & Meth. Phys. Res.* A272 (1988) 364.

[2] J. Smolin, T. Katsouleas, C. Joshi, P. Davis, C. Pellegrini, "Design of a plasma wakefield accelerator experiment at UCLA," *Bul. Am. Phys. Soc.* to be publ. Nov. 1990. Cf., T. Katsouleas, J.J. Su, W.B. Mori, C. Joshi, J.M. Dawson, "A compact 100MeV accelerator based on plasma wakefields," *Microwave and Particle Beam Sources and Directed Energy Concepts,* H.E. Brandt, ed., Proc. SPIE 1061, pp. 428-433 (1989).

[3] K. Batchelor, H. Kirk, J. Sheehan, M. Woodle, and K. McDonald, *Proc. European Particle Accel. Conf.*, Rome, Italy, June 7-12, 1988; also, K. Batchelor, *et al., Proc. 1989 Particle Accel. Conf.*, Chicago, IL, p. 273.

[4] John S. Fraser and Richard L. Sheffield, *IEEE J. Quant. Elec.,* 23 (1987) 1489; J.S. Fraser, *et al.*, "Photocathodes in Accel. Applications," *Proc. 1987 IEEE Particle Accel. Conf.*, eds., E.R. Lindstrom and L.S. Taylor, Wash., D.C., pp. 1705-1709; and, Michael E. Jones and William Peter, "Theory and simulation of high-brightness electron beam production from laser-irradiated photocathodes in the presence of DC and RF electric fields," *6th Int'l. Conf. on High-Power Particle Beams,* Japan, 1986.

[5] Glen T. Bennett, private communication.

[6] K. Halbach and R.F. Holsinger, Particle Accelerators, 7 (1976) 213.

[7] K.T. McDonald, "Design of the laser-driven RF electron gun for the BNL Accelerator Test Facility," *IEEE Trans. Electron Devices,* ED-35 (1988) 2052.

[8] D.A. Swenson, "The plane-wave transformer linac structure," *European Particle Accel. Conf.*, Vol. 2, 1988, Rome, Italy, ed. S. Tazzari, pp. 1418-1420.

[9] IEEE Proc. Vol. 127, Pt. B, No. 6 (1980).

[10] K.-Y. Ng, "Fields, Impedances, and Structures," in *Phys. of Part. Accelerators,* Vol. One, eds., M. Month and M. Dienes, AIP Conf. Proc. No. 184 (Am. Inst. of Physics, New York, 1989), pp. 472-524; especially §4.3 on beam position monitors.

[11] D.P. Russell. and K.T. McDonald, "A beam-profile monitor for the BNL Accelerator Test Facility (ATF)," *Proc. 1989 IEEE Particle Accel. Conf.*, Vol. 3, eds., F. Bennett and J. Kopta, Chicago, IL., pp. 1510-1512.

[12] K.T. McDonald and D.P. Russell, "Methods of Emittance Measurement," in the *Proc. of the Jont US-CERN School on Observation, Diagnosis and Correction in Part. Beams,* Capri, Italy, October 20-26, 1988.

[13] T.M. Tran and J.S. Wurtele, "Review of free-electron laser (FEL) simulation techniques," submitted for publication (Jan 1990) in *Computer Physics Reports.*